Data-Driven Gas Sensing Analysis of MgO Thin Films

Shams Nassif Jassem[1], Hussein Hassan Magli[2], Rushdi Ibrahim Jasim[3],
Wathiq Ayoub Taha Al Ramdhan[4] and Hadi Ahmed Hussin[3]
[1]*Nanotechnology and Advanced Materials Research Center, University of Technology, 10066 Baghdad, Iraq*
[2]*General Directorate of Education in Al-Qadisiyah Governorate, Ministry of Education, 58001 Al-Diwaniyah, Iraq*
[3]*Department of Physics, College of Education, Mustansiriyah University, 10052 Baghdad, Iraq*
[4]*Department of Medical Physics, Al-Manara College for Medical Sciences, 62001 Amarah, Iraq*
shams@uotechnology.edu.iq, hassanhafyaa@gmail.com, rushdi77@uomustansiriyah.edu.iq,
wathiq.alramdhan@uomanara.edu.iq, hadi.ahmed@uomustansiriayh.edu.iq

Keywords: MgO Thin Films, Spray Pyrolysis, Thermal Annealing, Structural Properties, Optical Characteristics, NO_2 Gas Sensor.

Abstract: This investigation provides a thorough assessment of the physical and gas-sensing characteristics of MgO thin coatings that were produced through chemical spray pyrolysis (CSP). XRD analysis confirmed the formation of a face-centred cubic (FCC) structure. The grain size increased from 11.82 nm to 13.43 nm with rising annealing temperature, while dislocation density decreased from 86.52 to 72.61 x 10^{14} lines/m², indicating improved crystallinity. Morphological analysis using AFM and SEM revealed a temperature-induced evolution from flat islands to well-defined spherical nano-grains. Surface roughness (R_a) decreased from 10.19 nm to 4.82 nm, and particle size was reduced from 93.2 nm to 46.5 nm. Optically, the films exhibited high transparency, with a visible transmittance of 95.9% at 400°C, which decreased slightly with increasing temperature due to increased light scattering. The optical bandgap decreased from 3.86 eV to 3.75 eV. The extinction coefficient at 400 nm declined from 0.70 to 0.61. Gas sensing results showed that the film annealed at 500°C exhibited the highest NO_2 response (26.5% at 150 ppm). However, sensitivity decreased at higher temperatures due to reduced surface defects and active adsorption sites.

1 INTRODUCTION

MgO crystallizes in a face-centered cubic (FCC) structure [1]. Due to its strong ionic bonds and significant electrostatic interactions between ions, MgO is classified as an ionic crystal [2], [3]. It possesses several properties, including high electrical resistance, chemical inertness, low thermal conductivity, high optical transparency, and mechanical durability [4]-[7]. Magnesium Oxide (MgO) is a versatile ceramic material renowned for its non-toxic nature, exceptional chemical stability, and robust physical properties. Its face-centered cubic (FCC) crystal structure, composed of Mg^{2+} (group IIA) and O^{2-} (group VIA) ions, contributes to its high thermal and mechanical stability. MgO exhibits outstanding antibacterial, antimicrobial, and photocatalytic properties, making it valuable for biomedical and environmental applications [1], [3], [5], [8]-[10]. The synthesis of MgO thin films has been accomplished through multiple deposition approaches, such as:sol-gel methods [4], [11]-[13], reactive sputtering [14], laser ablation [15], CVD [16], PLD [17] and (CSP) [18]. This research presents a comprehensive investigation of MgO thin films deposited by CSP, analyzing their structural, morphological, optical properties and NO_2 gas sensing capabilities. The spray pyrolysis method was selected for its ability to produce high-quality films with precise control over critical parameters, including thickness, density, and film uniformity [19].

2 EXPERIMENTAL

MgO thin films were fabricated via spray pyrolysis deposition. The initial solution was generated by dissolving magnesium trichloride ($MgCl_3$) in distilled water reaching a concentration of 0.05 M. Base substrates were coated with films. over 9 minutes. To enhance film quality, multilayer samples underwent a two-stage annealing process: initial pre-annealing at 400°C followed by post-annealing at either 450°C or

500°C for one hour. Film thickness, determined through gravimetric analysis, averaged 340 ± 25 nm. The structural features were assessed through XRD. Optical properties were evaluated using a JASCO UV/VIS/NIR V570 spectrophotometer. For gas sensing evaluation, resistance changes upon NO_2 exposure were measured in a custom-built cylindrical test chamber (16 cm in height and 8 cm in radius).

3 RESULTS AND DISCUSSIONS

The structural characteristics of the synthesized MgO thin films are presented in Figure 1 through their X-ray diffraction (XRD) patterns. These patterns display three distinct diffraction peaks located at 37.65°, 42.71°, and 62.71°, which correspond to the (111), (200), and (220) crystallographic planes, respectively [20]. The obtained diffraction data are in strong agreement with the standard JCPDS card No. 01-075-0477, confirming the successful formation of a polycrystalline MgO phase with a face-centered cubic (FCC) crystal structure. The sharp and well-defined nature of the peaks indicates high crystallinity and excellent phase purity of the deposited films. Notably, the (111) reflection exhibits the highest intensity, implying a preferred growth orientation along this plane, which is consistent with earlier reported studies on MgO thin films [21], [22]. This preferential orientation is significant, as it strongly influences the surface characteristics and functional performance of the material.

The crystallite size (D) was estimated using Scherrer's equation [23], [24], where K = 0.89, λ is the X-ray wavelength, β is the full width at half maximum, and θ is the Bragg angle. The results show that D increases from 11.82 nm to 13.43 nm with increasing annealing temperature, as summarized in the corresponding table. This trend confirms that thermal treatment promotes grain growth through enhanced atomic diffusion and crystallite coalescence, leading to reduced grain boundary density and improved structural ordering, in agreement with earlier reports [14], [17].

The dislocation density (δ) was calculated using the standard relation [25], [26], where δ is inversely proportional to the square of crystallite size. The obtained values for the annealed films (400–500 °C) are 86.52, 72.61, and 72.61 × 10^{14} lines/m², respectively [10], [27]. The observed reduction in dislocation density with increasing annealing temperature indicates a decrease in crystal defects. This improvement is attributed to thermally activated atomic rearrangement, which facilitates the formation of a more ordered and stable lattice structure. The nearly identical values at 450 °C and 500 °C suggest that defect reduction approaches a saturation limit at higher temperatures, where further thermal treatment produces minimal additional improvement [28].

The lattice strain (ε) was determined using the corresponding relation [29], [30]. The calculated values are 34.72, 29.85, and 28.13 × 10^{-4} for films annealed at 400 °C, 450 °C, and 500 °C, respectively [11], [24]. The gradual decrease in strain with increasing annealing temperature reflects a progressive relaxation of internal stresses and improved lattice stability. This behavior is consistent with the reduction in dislocation density and confirms enhanced crystalline quality with thermal treatment. A comprehensive summary of structural parameters, including FWHM, D, δ, and ε, as a function of annealing temperature is provided in Table 1 and Figure 2.

Figure 3 presents AFM images of MgO thin films annealed at 400–500 °C, scanned over an area of 10 × 10 μm. The micrographs (a1–a3) show uniformly distributed grains with a nearly spherical morphology across all samples, indicating a homogeneous surface structure. With increasing annealing temperature, a noticeable evolution in grain size and surface texture is observed, reflecting enhanced grain growth and surface reorganization. As shown in Table 2, the average particle size increases from 46.5 nm to 93.2 nm, confirming significant grain coalescence at higher temperatures. In addition, the average roughness (Ra) varies from 4.82 nm to 10.19 nm, while the root mean square roughness (RMS) ranges from 3.32 nm to 8.71 nm. These changes indicate a temperature-dependent modification of surface morphology, where increased atomic mobility at higher annealing temperatures promotes grain growth and surface restructuring [31], [32].

Table 1: *D*, E_g and S_P of the intended films.

Sample (°C)	2 θ (°)	(hkl) Plane	FWHM (°)	E_g (eV)	*D* (nm)	δ (× 10^{14}) (lines/m^2)	ε (× 10^{-4})
400	37.65	111	0.83	3.86	11.82	86.52	34.72
450	37.61	111	0.79	3.82	12.43	77.34	29.85
500	37.55	111	0.75	3.75	13.71	72.61	28.13

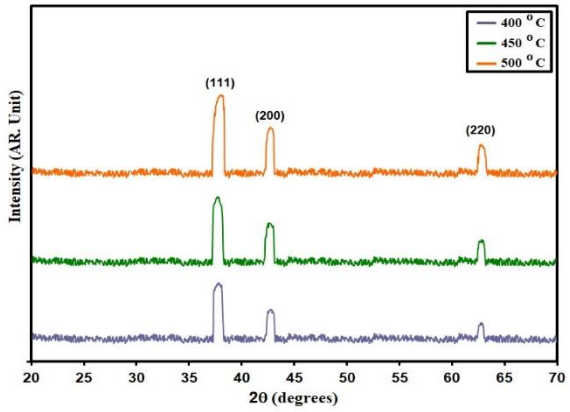

Figure 1: XRD styles of the intended films.

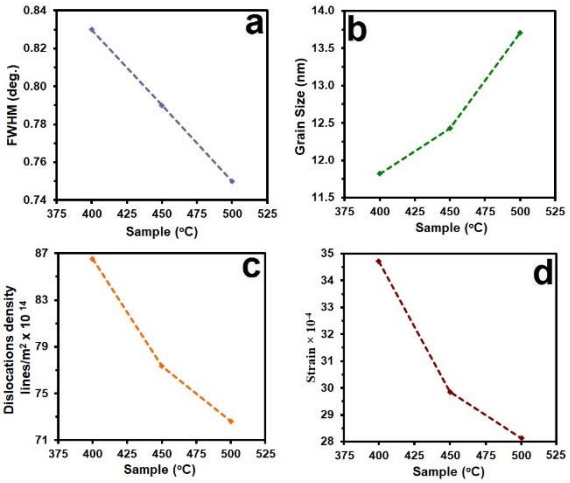

Figure 2: SP of the intended films.

As illustrated in Figure 4, the annealing temperature (AT) significantly influences the optical transmittance (T) of the MgO thin films [4]. All samples demonstrate high transparency within the visible range; however, the maximum transmittance decreases from 95.9% for the film annealed at 400 °C to 89.3% for the sample annealed at 500 °C. A consistent decreasing trend in transmittance is observed with increasing annealing temperature across all films. This behavior is mainly attributed to enhanced surface roughness and increased light scattering, which arise from the development of columnar grains with needle-like and rod-like morphologies at higher temperatures [33]. As the surface becomes rougher, the scattering of incident light increases, leading to a reduction in overall transparency [34], [35].

The relationship between absorbance (A) and transmittance (T) is defined by the standard optical expression [36], [37], where absorbance is directly related to the logarithmic inverse of transmittance. The corresponding form of this relation is given in Equation (4), where I_0 and I represent the incident and transmitted light intensities, respectively. As shown in Figure 5, absorbance increases with increasing annealing temperature. This enhancement is primarily associated with the growth in particle size and improved crystallinity of the films. The sample annealed at 500 °C exhibits the highest absorbance among all films [38], [39]. In addition, a slight red shift in the absorption edge is observed with increasing annealing temperature, which is commonly linked to crystallite enlargement and corresponding modifications in the electronic band structure, leading to a reduction in the optical bandgap [40], [41].

The absorption coefficient (α) was determined using the standard relation [42], [43], where film thickness is taken into account. The calculated values, shown in Figure 6, indicate that α increases significantly in the ultraviolet region and gradually decreases toward higher wavelengths. Furthermore, the absorption coefficient increases with annealing temperature, reaching values above 10^4 cm^{-1} [44], [45]. This enhancement in α suggests improved light–matter interaction due to microstructural evolution such as increased crystallinity and grain growth. The high absorption in the UV region confirms that MgO thin films are effective UV-absorbing materials, making them suitable for applications such as UV filtering and photodetection [46], [47].

Table 2: AFM parameters of deposit films.

Sample (°C)	P_{av} (nm)	R_a (nm)	RMS (m)
400	93.2	10.19	8.71
450	73.0	9.15	4.25
500	46.5	4.82	3.32

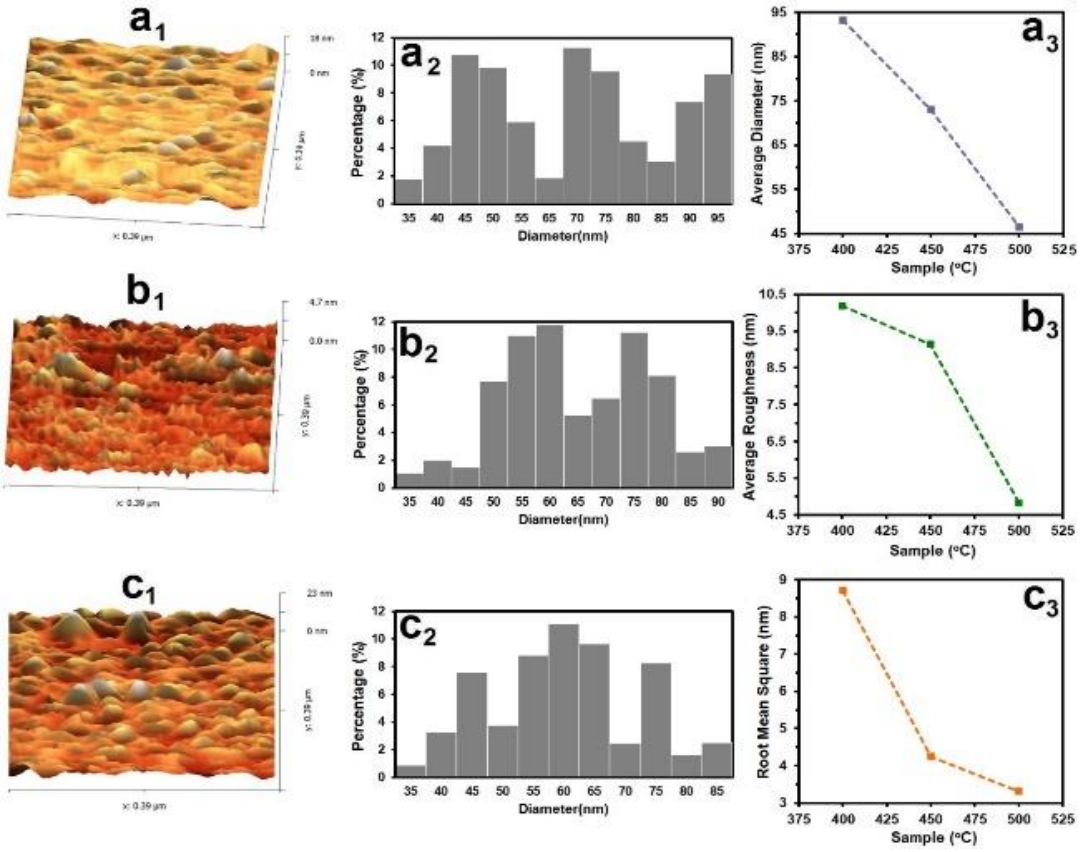

Figure 3: AFM images of MgO thin films annealed at different temperatures.

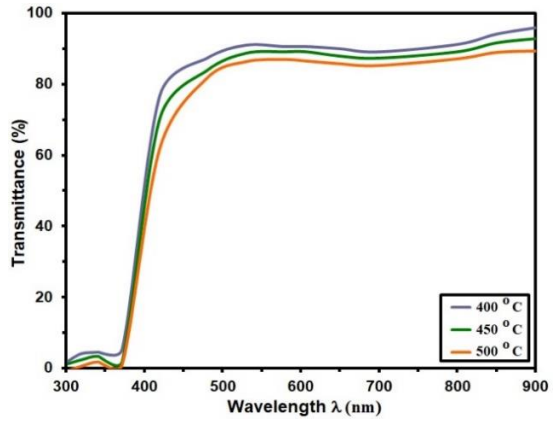

Figure 4: T of the intended films.

The optical band gap (Eg) of the MgO thin films was determined using Tauc's relation for direct allowed transitions [48], [49]. This approach relates the absorption coefficient and photon energy through a power-law dependence involving the band gap energy. The corresponding results are presented in Figure 7, which shows a gradual decrease in Eg with increasing annealing temperature. The extracted values are 3.86 eV, 3.82 eV, and 3.75 eV for films annealed at 400 °C, 450 °C, and 500 °C, respectively, consistent with previously reported values for MgO thin films prepared by different deposition techniques [50], [51]. The reduction in band gap with higher annealing temperature can be associated with improved crystallinity, increased grain size, and a reduction in defect states within the film. As the crystallite size increases, quantum confinement effects become weaker, resulting in a slight narrowing of the optical band gap. This behavior indicates that thermal treatment enhances structural ordering, which directly influences the optical properties of the films.

The extinction coefficient (k) was calculated using the standard optical relation [52], [13], which links it to the absorption coefficient and wavelength. The spectral dependence of k is shown in Figure 8, where a similar trend is observed between k and wavelength across all samples. The results also highlight the influence of annealing temperature on the extinction coefficient in the visible region [53], [54]. At a wavelength of 400 nm, k decreases from 0.70 for the film annealed at 400 °C to 0.64 at 450 °C

and 0.61 at 500 °C. This clear decreasing trend indicates that higher annealing temperatures lead to reduced optical losses, making the films more transparent. The reduction in k is mainly attributed to improved crystallinity and a lower concentration of structural defects, which collectively reduce light absorption and scattering. As a result, thermal annealing enhances the optical quality of the films, lowering the extinction coefficient and improving their suitability for optoelectronic applications [55], [56], [57], [58].

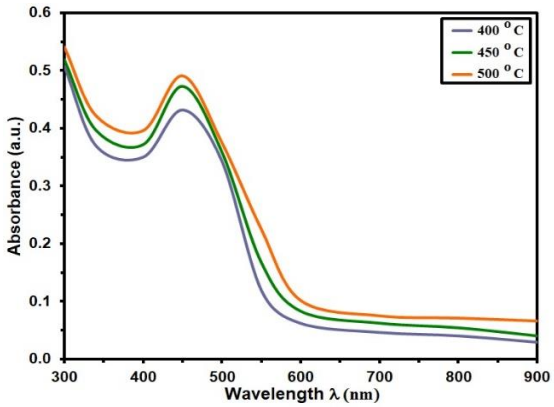

Figure 5: Absorbance of the intended films.

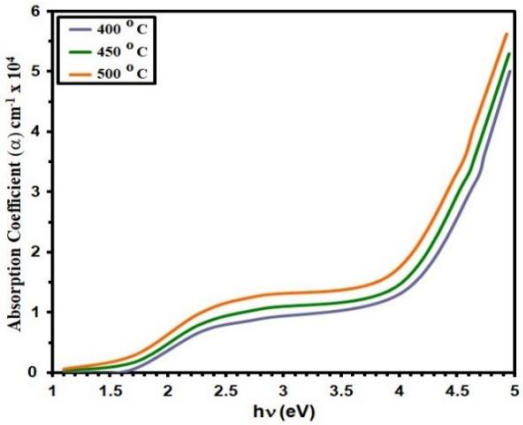

Figure 6: α of deposit films.

The refractive index (n) was evaluated using the standard optical relation [57], [58], which incorporates both reflectance and extinction coefficient. The corresponding expression accounts for the combined influence of surface reflection and absorption losses on the optical response of the material. The variation of n with annealing temperature is presented in Figure 9. At a wavelength of 450 nm, the refractive index values are found to be 3.38, 3.30, and 3.21 for films annealed at 400 °C, 450 °C, and 500 °C, respectively [59], [60]. A clear decreasing trend is observed with increasing annealing temperature, which can be explained by microstructural evolution induced by thermal treatment. Grain growth, reduced defect concentration, and changes in packing density lead to a less optically dense material, thereby lowering the refractive index [61], [62].

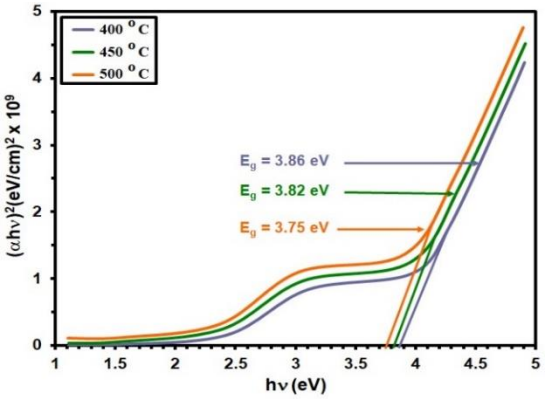

Figure 7: $(\alpha h\nu)^2$ of the intended films.

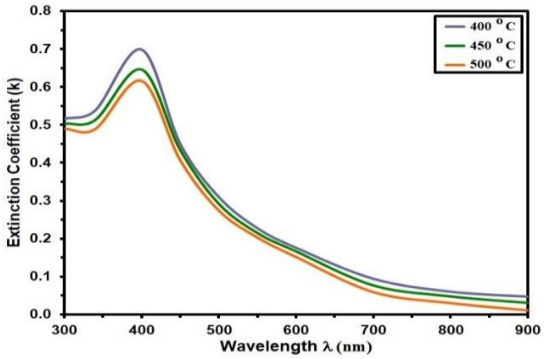

Figure 8: k of the deposit films.

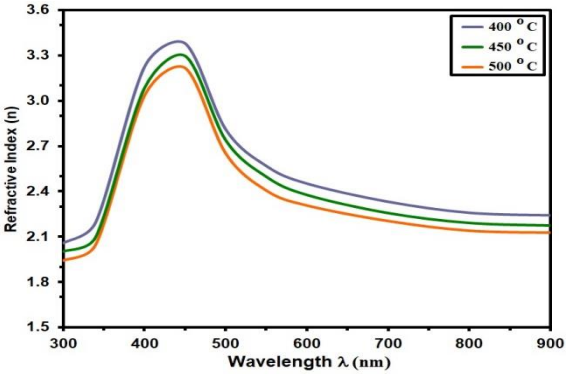

Figure 9: n of the deposit films.

The gas sensing response (sensitivity) was calculated using the standard expression [63], [64], which describes the relative change in electrical resistance upon exposure to the target gas. In this relation, $R_a$represents the resistance in the presence of NO_2, while $R_g$denotes the baseline resistance in air. The time-dependent resistance behavior of MgO thin films annealed at 400 °C, 450 °C, and 500 °C under NO_2 exposure at 100 °C is shown in Figure 10 [63], [64]. When exposed to NO_2, oxidation processes occur on the film surface, where adsorbed oxygen species release electrons back into the conduction band, resulting in an increase in resistance due to the formation of higher potential barriers at grain boundaries [65], [66]. Among all samples, the film annealed at 500 °C exhibits the strongest resistance response, indicating improved sensing behavior. This enhanced response is associated with increased surface activity and modified grain boundary characteristics, which facilitate stronger interaction with gas molecules.

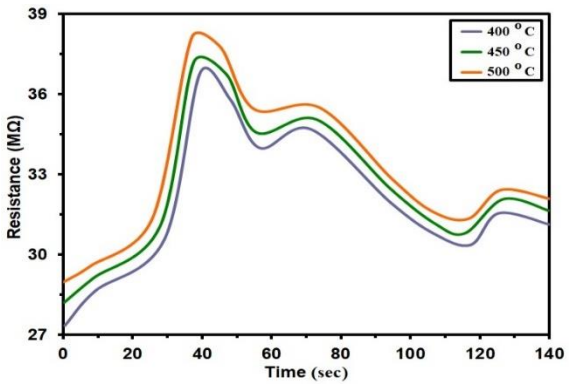

Figure 10: The sensitivity (S) of MgO thin films versus operating time for samples annealed at 400, 450, and 500°C.

Figure 11 presents the sensitivity of MgO thin films toward NO_2 gas as a function of annealing temperature in the range of 400–500 °C. The results show a gradual decrease in sensitivity with increasing annealing temperature, which is mainly attributed to enhanced charge carrier recombination and reduced density of surface defects. Quantitatively, the sensitivity decreases from 24.1% to 10.6% at 50 ppm, from 25.3% to 11.4% at 100 ppm, and from 26.5% to 12.6% at 150 ppm. This reduction indicates that higher annealing temperatures promote grain growth and decrease the number of active adsorption sites, thereby limiting gas–surface interactions. As a result, although annealing improves crystallinity and structural stability, it simultaneously reduces the overall gas sensing sensitivity due to diminished surface reactivity [67].

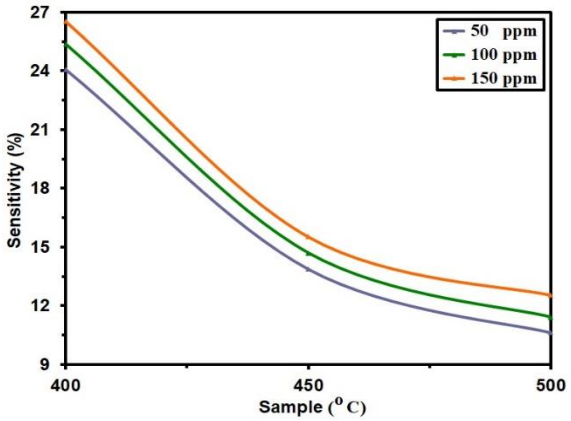

Figure 11: Sensitivity of MgO annealed at (400, 450 and 500) °C.

4 CONCLUSIONS

This study thoroughly examined the impact of annealing temperature of nanostructured MgO thin films deposit by CSP. XRD analysis is verified via the formation of a face-centered cubic (FCC) structure. As the AT increased from 400°C to 500°C, grain size grew from 11.82 nm to 13.43 nm. Dislocation density and microstrain decreased with higher AT. Morphological studies using AFM Surface roughness (R_a) dropped from 10.19 nm to 4.82 nm, and average particle size decreased from 93.2 nm to 46.5 nm. Optically, the films demonstrated high transparency in the visible range, with transmittance declining slightly from 95.9% at 400°C to 89.3% at 500°C due to increased light scattering. The optical bandgap narrowed from 3.86 eV to 3.75 eV. Both extinction coefficient and refractive index decreased with higher annealing temperatures. Regarding gas sensing, the MgO film annealed at 500°C exhibited the highest sensitivity (26.5% at 150 ppm NO_2), attributed to enhanced surface reactivity and potential barriers at grain boundaries. However, sensitivity declined at higher annealing due to fewer surface defects and active adsorption sites.

ACKNOWLEDGMENTS

This research was supported by Mustansiriyah University (www.uomustansiriyah.edu.iq).

REFERENCES

[1] S. Aksay, "Effects of Al dopant on XRD, FT-IR and UV-vis properties of MgO films," Physica B, vol. 570, pp. 280-284, 2019.

[2] A.M.E. Raj, M. Jayachandran and C. Sanjeeviraja, "Fabrication techniques and material properties of dielectric MgO thin films - a status review," CIRP J. Manuf. Sci. Technol., vol. 2, no. 2, pp. 92-113, 2010.

[3] M. Tlili, C. Nefzi, B. Alhalaili, C. Bouzidi, L. Ajili, N. Jebbari and N. Turki Kamoun, "Synthesis and characterization of MgO thin films obtained by spray technique for optoelectronic applications," Nanomaterials, vol. 11, no. 11, 3076, 2021.

[4] H. Zulkefle, L.N. Ismail, R.A. Bakar and M.R. Mahmood, "Molar concentration effect on MgO thin films properties," in Proc. IEEE Symp. Ind. Electron. Appl., pp. 468-471, 2011.

[5] A. Taşer, M. Gulduren and H. Guney, "Cr dopant effect on MgO thin film structural, optical and morphology properties," Erzincan Univ. J. Sci. Technol., vol. 14, no. 1, pp. 284-291, 2021.

[6] G.H. Reiling and E.B. Hensley, "Fundamental optical absorption in magnesium oxide," Phys. Rev., vol. 112, pp. 1106-1111, 1958.

[7] F. Şenaslan, A. Celik and M. Taşdemir, "Production of high transparent MgO films by radio-frequency sputtering method," Gumuşhane Univ. J. Sci., vol. 12, no. 1, pp. 320-326, 2022.

[8] K.V. Rao and C.S. Sunandana, "Structure and microstructure of combustion synthesized MgO nanoparticles," J. Mater. Sci., vol. 43, pp. 146-154, 2008.

[9] J.P. Singh, V. Singh, A. Sharma, G. Pandey and K.H. Chae, "Approaches to synthesize MgO nanostructures for diverse applications," Heliyon, vol. 6, e04882, 2020.

[10] S.P. Ghorbanzade Zaferani, N. Nabian, M. Delavar and S.M. Rabiee, "Direct impregnation of MgO nanoparticles in bioactive glass," Iran. J. Sci. Technol., vol. 45, no. 3, pp. 885-898, 2021.

[11] R. Wahab, S. Ansari, M. Dar, Y.S. Kim and H.S. Shin, "Synthesis of magnesium oxide nanoparticles by sol-gel process," Mater. Sci. Forum, pp. 983-986, 2007, doi: 10.4028/www.scientific.net/MSF.558-559.983.

[12] I.C. Ho, Y. Xu and J.D. Mackenzie, "Electrical and optical properties of MgO thin film prepared by sol-gel technique," J. Sol-Gel Sci. Technol., vol. 9, pp. 295-301, 1997.

[13] Y.W. Choi and J. Kim, "Reactive sputtering of magnesium oxide thin film," Thin Solid Films, vol. 460, pp. 295-299, 2004.

[14] P. Płóciennik, D. Guichaoua, A. Zawadzka, A. Korcala, J. Strzelecki, P. Trzaska and B. Sahraoui, "Optical properties of MgO thin films grown by laser ablation technique," Opt. Quantum Electron., vol. 48, 277, 2016, doi: 10.1007/s11082-016-0536-8.

[15] G. Carta, N. El Habra, L. Crociani, G. Rossetto, P. Zanella, G. Paolucci, D. Barreca and E. Tondello, "CVD of MgO thin films," Chem. Vap. Depos., vol. 13, pp. 185-189, 2007, doi: 10.1002/cvde.200606574.

[16] S. Kaneko, T. Ito, M. Soga, Y. Motoizumi, M. Yasui, Y. Hirabayashi, T. Ozawa and M. Yoshimoto, "Growth of nanocubic MgO on silicon substrate," Jpn. J. Appl. Phys., vol. 52, 01AN02, 2013, doi: 10.7567/JJAP.52.01AN02.

[17] F. Niu, B.H. Hoerman and B.W. Wessels, "Metalorganic molecular beam epitaxy of magnesium oxide on silicon," MRS Proc., vol. 619, pp. 149-154, 2000, doi: 10.1557/PROC-619-149.

[18] M. Tlili, N. Jebbari, W. Naffouti and N.T. Kamoun, "Effect of precursor nature on physical properties of chemically sprayed MgO thin films," Eur. Phys. J. Plus, vol. 135, pp. 1-12, 2020.

[19] S.S. Li, Semiconductor Physical Electronics, New York, NY, USA: Springer, 2006.

[20] G. Song, Y. Wang and D.Q. Tan, "A review of surface roughness impact on dielectric film properties," IET Nanodielectrics, vol. 5, no. 1, pp. 1-23, 2022.

[21] W.J. Liu, Y.H. Chang, S.T. Hsu, C.L. Fern, Y.T. Chen, S.Y. Tsao and S.H. Lin, "Exploring correlation between surface roughness and properties of thin films," J. Electron. Mater., vol. 53, pp. 1-14, 2024.

[22] N.N. Jandow, N.F. Habubi, S.S. Chiad, I.A. Al-Baidhany and M.A. Qaeed, "Annealing effects on optical parameters of Fe2O3:Ni thin films," Int. J. Nanoelectron. Mater., vol. 12, no. 1, pp. 1-10, 2019.

[23] S. Sagadevan, S. Venilla, A.R. Marlinda, M. Johan, Y.A. Wahab, R. Zakaria and N. Ahmad, "Effect of synthesis temperature on MgO nanostructures," J. Nanosci. Nanotechnol., vol. 20, no. 4, pp. 2488-2494, 2020.

[24] R. Kuekha, T.H. Mubarak and B. Azhdar, "Electromagnetic interference shielding of nanoferrites," Adv. Mater. Sci. Eng., 2022, 3992402.

[25] B.A. Bader, S.K. Muhammad, A.M. Jabbar, K.H. Abass, S.S. Chiad and N.F. Habubi, "Synthesis and characterization of indium-doped CdO nanostructured thin films," J. Nanostruct., vol. 10, no. 4, pp. 744-750, 2020.

[26] D.L. Wood and J. Tauc, "Weak absorption tails in amorphous semiconductors," Phys. Rev. B, vol. 5, no. 8, p. 3144, 1972.

[27] A. Ait Hssi, L. Atourki, N. Labchir, M. Ouafi, K. Abouabassi, A. Elfanaoui and A. Ihlal, "Optical and dielectric properties of Cu2O films," Mater. Res. Express, vol. 7, 016424, 2020.

[28] S. Thirumavalavan, K. Mani and S. Sagadevan, "Investigation of copper selenide thin films," Mater. Res., vol. 18, pp. 1000-1007, 2015.

[29] N.F. Habubi, K.H. Abass, S.S. Chiad, D.M.A. Latif, J.N. Nidhal and A.I. Al-Baidhany, "Dispersion parameters of PVA films doped with Fe," J. Phys.: Conf. Ser., vol. 1003, 012094, 2018.

[30] B. Thangaraju and P. Kaliannan, "Polycrystalline lead tin chalcogenide thin film," Cryst. Res. Technol., vol. 35, no. 1, pp. 71-75, 2000.

[31] K.R. Rajesh and C.S. Menon, "Electrical and optical properties of MnPc thin films," Eur. Phys. J. B, vol. 47, pp. 171-176, 2005.

[32] M.H. Shinen, S.A.A. AlSaati and F.Z. Razooqi, "Preparation of TiO2 thin films," J. Phys., vol. 1032, 012018, 2018.

[33] V.S. Stepanyuk, A. Szasz and B.L. Grigorenko, "Electronic structure and optical properties of MgO," Phys. Status Solidi, vol. 155, pp. 179-184, 1989.

[34] Y. Benkrima, A. Souigat, A. Achouri, M.E. Soudani, Y. Chaouche, Z. Korichi and D. Slimani, "DFT study of MgO properties," J. Nano Electron. Phys., vol. 14, no. 1, pp. 01003-1-01003-5, 2022.

[35] W.A. Aelawi, S. Alptekin and M.H. Al-Timimi, "Structural, optical and electrical properties of CdS1−xCuxS films," Indian J. Phys., vol. 97, no. 13, pp. 3949-3956, 2023.

[36] M. Myvizhi, K.S. Kumar, P.R. Kavitha and P. Selvakumar, "Structure and optoelectronic properties of MgO nanocrystals," J. Ovonic Res., vol. 19, no. 3, pp. 265-273, 2023.

[37] J. Tauc, Amorphous and Liquid Semiconductors, Heidelberg, Germany: Springer, 2012.

[38] T. Sertel, Y. Ozen, A. Tataroglu, T. Asar, S.S. Cetin and S. Ozcelik, "Electrical properties of GaAsPN/GaPN diode," J. Electron. Mater., vol. 46, pp. 4590-4595, 2017.

[39] S.S. Chiad, A.S. Alkelaby and K.S. Sharba, "Optical conduct of Co3O4 nanostructures," J. Glob. Pharma Technol., vol. 11, no. 7, pp. 662-665, 2020.

[40] O. Gullu and A. Tataroğlu, "Production of chromium oxide thin layers," Phys. Scr., vol. 98, 015837, 2022.

[41] H. Seymen and Ş. Karataş, "Analysis of electrical characteristics of Al/GO-PTCDA/p-Si," J. Mater. Electron. Devices, vol. 6, no. 1, pp. 28-32, 2021.

[42] D.S. Reddy, V. Janardhanam, V.R. Reddy and C.J. Choi, "Modification of interface properties of Au/n-GaN junction," Vacuum, vol. 215, 112300, 2023.

[43] H. Norde, "A modified forward I-V plot for Schottky diodes," J. Appl. Phys., vol. 50, no. 7, pp. 5052-5053, 1979.

[44] A. Buyukbas-Ulusan and A. Tataroglu, "Electrical characterization of MIS diode," J. Mater. Sci. Mater. Electron., vol. 31, pp. 9888-9893, 2020.

[45] S.S. Chiad, H.A. Noor, O.M. Abdulmunem and N.F. Habubi, "Optical and structural properties of Ni-doped Co3O4 films," J. Phys.: Conf. Ser., vol. 1362, 2019.

[46] D.E. Yıldız, H.H. Gullu and H.K. Cavus, "Effect of TiO2 thin film with dopants," J. Inorg. Organomet. Polym. Mater., vol. 32, no. 3, pp. 1067-1077, 2022.

[47] G.A. Aydemir, D. Akay, A. Tataroğlu and S.B. Ocak, "Electrical and optical properties of p-Si structures," Mater. Sci. Eng. B, vol. 294, 116552, 2023.

[48] D. Caceres, I. Colera, I. Vergara, R. Gonzalez and E. Roman, "Characterization of MgO thin films," Vacuum, vol. 67, no. 3-4, pp. 577-581, 2002.

[49] R.I. Jasim, E.H. Hadi, S.S. Chiad, N.F. Habubi, M. Jadan and J.S. Addasi, "Effect of silver doping on CdSe thin films," J. Ovonic Res., vol. 19, no. 2, pp. 187-196, 2023.

[50] H. Guney and D. İskenderoğlu, "Synthesis of MgO thin films by SILAR technique," Ceram. Int., vol. 44, no. 7, pp. 7788-7793, 2018.

[51] H.İ. Efkere and S. Ozcelik, "Detailed analysis of WO3 nanostructure properties," J. Mater. Sci. Mater. Electron., vol. 34, no. 29, 2001, 2023.

[52] V.R. Reddy, P.S. Reddy, I.N. Reddy and C.J. Choi, "Microstructural and electrical properties of Au/NiO/n-GaN," RSC Adv., vol. 6, no. 107, pp. 105761-105770, 2016.

[53] Y. Badali, H. Altan and S. Altındal, "Thermal dependence on electrical characteristics," J. Mater. Sci. Mater. Electron., vol. 35, no. 3, pp. 1-10, 2024.

[54] A.A. Kamil, N.A. Bakr, T.H. Mubarak and J. Al-Zanqanawee, "Effect of nanoparticles on ZnO thin films," J. Ovonic Res., vol. 18, no. 3, pp. 431-442, 2022.

[55] S.S. Chiad, H.A. Noor, O.M. Abdulmunem, N.F. Habubi, M. Jadan and J.S. Addasi, "Optical and structural performance of Te thin films," J. Ovonic Res., vol. 16, no. 1, pp. 35-40, 2020.

[56] H. Uslu, Ş. Altındal, U.M.T. Aydemir, I. Dokme and I.M. Afandiyeva, "Interface states and series resistance effects," J. Alloys Compd., vol. 503, no. 1, pp. 96-102, 2010.

[57] C.Ş. Guclu, E.E. Tanrıkulu, A. Dere, Ş. Altındal and Y. Azizian-Kalandaragh, "Comparison of electrical characteristics of Schottky diodes," J. Mater. Sci. Mater. Electron., vol. 34, no. 28, 1909, 2023.

[58] H.K. Khanfar and A.F. Qasrawi, "Performance of Au/MgO/Ni photovoltaic devices," Mater. Sci. Semicond. Process., vol. 29, pp. 183-187, 2015.

[59] A. Eroğlu, S. Demirezen, Y. Azizian-Kalandaragh and Ş. Altındal, "Comparative study on electrical properties of Schottky diodes," J. Mater. Sci. Mater. Electron., vol. 31, pp. 14466-14477, 2020.

[60] G.B. Yildirim and E. Daş, "Synthesis of MgO-graphene nanocomposites," Phys. Scr., vol. 98, no. 8, 085911, 2023.

[61] H.C. Card and E.H. Rhoderick, "Studies of tunnel MOS diodes," J. Phys. D, vol. 4, no. 10, p. 1589, 1971.

[62] E.H. Rhoderick and R.H. Williams, Metal-Semiconductor Contacts, Oxford, UK: Clarendon Press, 1988.

[63] C. Yang, H. Chen and C. Guan, "Hybrid CoO nanowires for energy storage devices," Nanomaterials, vol. 9, 586, 2019.

[64] Y.C. Liang, Y.C. Chang and W.C. Zhao, "Design of ZnO-NiO composite nanosheets," Nanomaterials, vol. 10, 1989, 2020.

[65] J. Green, "Calcination of Mg(OH)2 to active MgO," J. Mater. Sci., vol. 18, pp. 637-651, 1983.

[66] A.A. Yaqoob, H. Ahmad, T. Parveen, A. Ahmad, M. Oves, I.M.I. Ismail, H.A. Qari, K. Umar and M.N. Mohamad Ibrahim, "Recent advances in metal decorated nanomaterials," Front. Chem., vol. 8, 341, 2020.

[67] P. Cousin and R.A. Ross, "Preparation of mixed oxides: a review," Mater. Sci. Eng. A, vol. 130, pp. 119-125, 1990.